A Systematic Computational Study on the Reactions of HO_2 with RO_2: The HO_2 + CH_3O_2(CD_3O_2) and HO_2 + CH_2FO_2 Reactions

Hua Hou and Baoshan Wang*

College of Chemistry and Molecular Sciences, Wuhan University, Wuhan 430072, People's Republic of China

Received: August 15, 2004; In Final Form: November 11, 2004

A systematic theoretical study of the reactions of HO_2 with RO_2 has been carried out. The major concern of the present work is to gain insight into the reaction mechanism and then to explain experimental observations and to predict new product channels for this class of reactions of importance in the atmosphere. In this paper, the reaction mechanisms for two reactions, namely, HO_2 + CH_3O_2 and HO_2 + CH_2FO_2, are reported. Both singlet and triplet potential energy surfaces are investigated. The complexity of the present system makes it impossible to use a single ab initio method to map out all the reaction paths. Various ab initio methods including MP2, CISD, QCISD(T), CCSD(T), CASSCF, and density function theory (B3LYP) have been employed with the basis sets ranging from 6-31G(d) to an extrapolated complete basis set (CBS) limit. It has been established that the CCSD(T)/cc-pVDZ//B3LYP/6-311G(d,p) scheme represents the most feasible method for our systematic study. For the HO_2 + CH_3O_2 reaction, the production of CH_3OOH is determined to be the dominant channel. For the HO_2 + CH_2FO_2 reaction, both CH_2FOOH and CHFO are major products, whereas the formation of CHFO is dominant in the overall reaction. The computational findings give a fair explanation for the experimental observation of the products.

I. Introduction

The reactions of HO_2 with the organic peroxy radicals (RO_2) are important atmospheric degradation pathways for organic compounds under low NO_x conditions in the global or regional environment. Moreover, these reactions represent an important chemical sink for the HO_x radicals in the troposphere.[1,2] Experimentally, the stable products formed in the HO_2 + RO_2 reactions have been studied extensively by Wallington, Orlando, Tyndall, and Hasson et al.[3−22] The available product information is summarized in Table 1. It has been found that the reaction between HO_2 and RO_2 proceeds via two distinct channels, giving either hydroperoxide (ROOH) or carbonyl products. More interestingly, the reactions of HO_2 with the unsubstituted RO_2 radicals (e.g., CH_3O_2, $C_2H_5O_2$, etc.) produce only ROOH. In contrast, the reactions between HO_2 and the substituted RO_2 (e.g., CH_2FO_2, CH_2ClO_2, $CHCl_2O_2$, and $CH_3OCH_2O_2$) produce both ROOH and carbonyl. The relative yields of the two products depend on the chemical identity of the R-group. There is no explanation for this substitution effect because the reaction mechanisms are unknown.

An ab initio computation is invaluable for gaining some insight into the reaction mechanism. To assess the likelihood of the occurrence of these processes, a systematic calculation that provides data on a whole suite of related radical reactions via the same method is extremely useful. Such self-consistent data sets have proven useful in the development of structure−reactivity relationships.[2] Therefore, we have calculated a total of 11 reactions [e.g., HO_2 + CH_3O_2, $C_2H_5O_2$, CH_2FO_2, CH_2ClO_2, $CHCl_2O_2$, CCl_3O_2, $HOCH_2O_2$, $CH_3OCH_2O_2$, $CH_3C(O)CH_2O_2$, $CH_3C(O)O_2$, and $C_2F_5C(O)O_2$] as listed in Table 1 systematically. To explain the experimentally observed ROOH and carbonyl products, Wallington et al.[3,11−22] proposed a few reaction mechanisms which include direct abstraction and concerted reactions with four- and six-membered transition states. However, no rigorous ab initio calculation has ever been done except that the MP2/6-31G(d,p) method was used to calculate the equilibrium geometries of CH_3O_2H and CH_2FO_2H.[11] In this paper, the reaction mechanisms for two reactions, HO_2 + CH_3O_2 and HO_2 + CH_2FO_2, are reported.

After a brief description of the computational methods in section II, the reaction mechanisms for the HO_2 + CH_3O_2 and HO_2 + CH_2FO_2 reactions are discussed in sections III.1 and III.2, respectively. The unimolecular decomposition of the ROOH (e.g., CH_3OOH and CH_2FOOH) products is investigated in section III.3. Section III.4 summarizes the characteristics of the tetroxide intermediates (RO_4H). The computational methods are validated in section III.5, and some conclusions are drawn in section VI.

II. Computational Methods

Geometrical parameters of the reactants, products, intermediates, and transition states were optimized using the density functional B3LYP[23] with the 6-311G(d,p) basis set unless otherwise stated. Harmonic vibrational frequencies calculated at the same level were used for the characterization of stationary points and zero-point energy (ZPE) corrections. A minimum has no imaginary frequency, and a transition state has only one imaginary frequency. Moreover, transition states were subjected to intrinsic reaction coordinate (IRC)[24] calculations to confirm the connection between reactants and products. It should be noted that a few IRC calculations failed due to a convergence problem. Alternatively, the displacement vector of the imaginary normal vibrational mode is used to identify the connection.[25,26] To improve the accuracy of the calculated barrier heights and heats of reaction, the CCSD(T)/cc-pVDZ method[27−31] was used to calculate the final energies at the B3LYP/6-311G(d,p)

* Corresponding author. E-mail: wangb@chem.whu.edu.cn. Fax: 86-27-68754067.

10.1021/jp046329e CCC: $30.25
Published on Web 12/30/2004

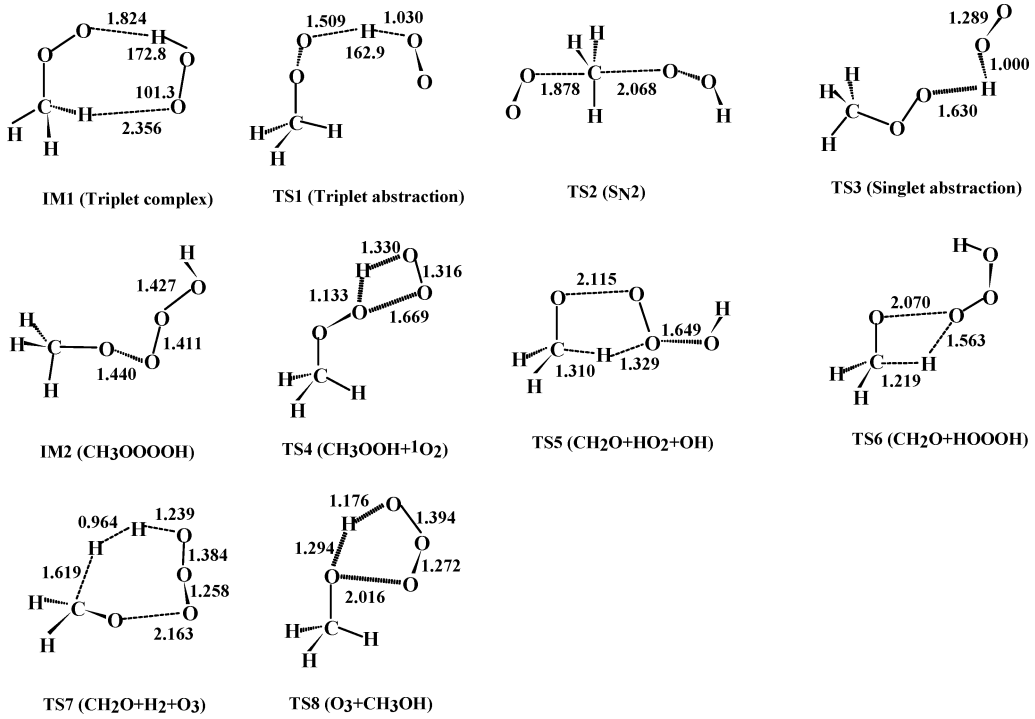

Figure 1. Optimized geometries of the transition states and intermediates involved in the $HO_2 + CH_3OO$ reaction at the B3LYP/6-311G(d,p) level of theory. The geometrical parameters for TS4 are obtained at the CISD/cc-pVDZ level.

TABLE 1: Summary of the Products Observed Experimentally for the $HO_2 + RO_2$ Reaction

type	RO_2	product (yield)		refs
unsubstituted	CH_3O_2, CD_3O_2			3−5
	$C_2H_5O_2$	only ROOH		6−8
	$C_5H_9O_2$, $C_6H_{11}O_2$	($\geq 0.9 \pm 0.1$)		9
	$(CH_3)_3CO_2$			10
substituted	CH_2FO_2	CH_2FOOH (0.29 ± 0.08)	CHFO (0.71 ± 0.11)	11
	CH_2ClO_2	CH_2ClOOH (0.27 ± 0.05)	CHClO (0.73 ± 0.12)	12
	$CHCl_2O_2$	CCl_2O (0.24)	CHClO (0.71)	13
	CCl_3O_2	CCl_2O (1.0)		13
	$HOCH_2O_2$	$HOCH_2OOH$ (0.60)	HCOOH (0.40)	14
	$CH_3OCH_2O_2$	CH_3OCH_2OOH (0.53 ± 0.08)	CH_3CHO (0.40 ± 0.04)	15
	$CH_3C(O)O_2$	$CH_3C(O)OOH$ (0.80)	CH_3COOH (0.20)	8, 16−20
	$CH_3C(O)CH_2O_2$	$CH_3C(O)CH_2OOH$ (0.33 ± 0.10)	$CH_3C(O)CH_2O$ (0.67 ± 0.20)	8, 21
	$C_2F_5C(O)O_2$	$C_2F_5C(O)OOH$ (0.76 ± 0.04)	C_2F_5COOH (0.24 ± 0.04)	22

optimized geometries. All ab initio calculations were carried out using the Gaussian 03 program.[32]

III. Results and Discussion

III.1. The $HO_2 + CH_3O_2$ Reaction. The structures of the intermediates and transition states involved in the $HO_2 + CH_3O_2$ reaction are shown in Figure 1. The schematic potential energy surface is shown in Figure 2. The energetic data are summarized in Table 2. As shown in Figure 2, the reaction occurs on both triplet and singlet surfaces. However, the transition states TS2, TS4, and TS7, leading to the products $CH_3OOH + {}^3O_2$, $CH_3OOH + {}^1O_2$, and $CH_2O + H_2 + O_3$, respectively, are well above the energy available in the reaction at normal temperatures and are thus not discussed further.

III.1.1. The Triplet Surface. As can be seen from Figure 2, direct hydrogen abstraction on the triplet surface possesses the lowest barrier. The energy of TS1 is even 3.8 kcal/mol lower than the total energy of the reactants. The forming OH bond is 1.509 Å, which is 0.54 Å longer than that in the product CH_3OOH. The breaking HO bond is 1.03 Å, which is only slightly longer by 0.06 Å than that of the HO_2 molecule. Evidently, TS1 is an early barrier, consistent with the reaction exothermicity of 37.82 kcal/mol. The seven-membered-ring hydrogen-bonding complex IM1 exits in the entrance channel along the reaction path. The binding energy is 7.65 kcal/mol.

III.1.2. The Singlet Surface. Both direct hydrogen abstraction and addition/elimination mechanisms are found on the singlet surface. The hydrogen abstraction proceeds via transition state TS3. The forming OH bond is 1.63 Å. The breaking HO bond is only slightly stretched to 1.00 Å, which is evidently a feature of the early barrier. Unlike TS1 for the triplet abstraction,

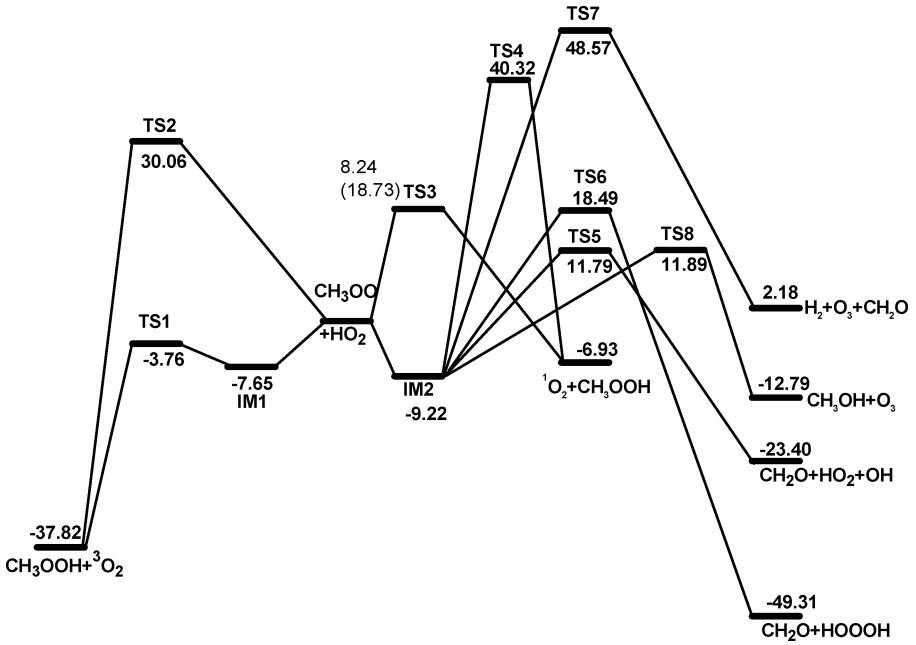

Figure 2. Schematic profile for the potential energy surface of the $HO_2 + CH_3OO$ reaction. The indicated energies (in kilocalories per mole) are calculated with the CCSD(T)/cc-pVDZ//B3LYP/6-311G(d,p) scheme. The value in parentheses for TS3 is calculated at the CCSD(T)/cc-pVDZ level but with the CISD/cc-pVDZ optimized geometry.

TABLE 2: Relative Energies Calculated at the CCSD(T)/cc-pVDZ Level with the B3LYP/6-311G(d,p) Optimized Geometries for the $HO_2 + CH_3OO$ (CD_3OO) Reaction[a]

species	ZPE	ZPE (D-substituted)	B3LYP/6-311G**	CCSD(T)/cc-pVDZ	exptl[b]
$HO_2 + CH_3OO$	35.72	29.51	0.0	0.0	0.0
IM1	37.56	31.13	−7.67	−7.65	
IM2	38.46	32.01	−6.45	−9.22	
TS1	36.05	29.66	−7.40	−3.76	
TS2	35.57	29.25	20.83	30.06	
TS3	36.79	30.68	24.37	8.24 (18.73)[c]	
TS4	37.22[c]	30.87[c]		40.32[c]	
TS5	34.26	28.79	14.68	11.79	
TS6	34.53	28.95	23.61	18.49	
TS7	31.76	26.19	50.0	48.57	
TS8	35.47	29.11	17.48	11.89	
$CH_3OOH + {}^3O_2$	36.49	30.30	−32.63	−37.82	−38. 4 ± 3.9
$CH_3OOH + {}^1O_2$	36.47	30.27	6.37	−6.93	
$CH_2O + HO_2 + OH$	30.78	25.13	−16.88	−23.40	−19.8 ± 2.9
$CH_2O + HOOOH$	35.65	29.72	−44.64	−49.31	−46.6 ± 4.0[d]
$CH_2O + H_2 + O_3$	27.50	23.07	14.07	2.18	2.0 ± 2.5
$CH_3OH + O_3$	36.64	30.62	−2.82	−12.79	−15.2 ± 2.6

[a] In kilocalories per mole. The total energy of $HO_2 + CH_3O_2$ is −341.222 25 and −340.306 92 (in hartrees) at the B3LYP/6-311G** and CCSD(T)/cc-pVDZ levels, respectively. [b] Using the enthalpies of formation from ref 33 and the references therein with the thermal correction at 298.15 K. [c] Calculated with the CISD/cc-pVDZ optimized geometry. [d] Using an upper-limit value of −26.0 kcal/mol for HOOOH in ref 34.

the OHO angle in TS3 is far from linearity with a value of 106.8°. The corresponding barrier height is 8.24 kcal/mol.

The addition (recombination) between the terminal oxygen atoms of the HO_2 and CH_3O_2 radicals leads to the intermediate IM2. As shown in Figure 2, the potential well of 9.2 kcal/mol is fairly shallow, being only slightly deeper than the hydrogen-bonding complex IM1.

IM2 decomposes into $CH_2O + HO_2 + OH$ via the five-membered-ring transition state TS5. Interestingly, this channel could be considered as a HO_2-mediated dissociation process of CH_3O_2, since HO_2 acts as a catalyst. As shown in Figure 1, the hydrogen is migrating from C to O to reproduce HO_2 while the remaining two OO bonds are breaking. The barrier for TS5 is 11.79 kcal/mol. The other path leading to formaldehyde involves the four-center transition state TS6. Although the formation of $CH_2O + HOOOH$ is more exothermic than $CH_2O + HO_2 + OH$, the energy of TS6 is 6.7 kcal/mol higher than that of TS5.

The reaction leading to methanol (CH_3OH) occurs via the five-membered-ring transition state TS8. As shown in Figure 1, the terminal hydrogen atom shifts to the last oxygen atom and the OO bond is broken simultaneously. The CH_3 group is just a speculator in the reaction. The energy of TS8 is very close to that of TS5. Thus, the formation of CH_3OH and CH_2O could be competitive.

In summary, the dominant product channel in the $CH_3O_2 + HO_2$ reaction may be determined straightforwardly according to the potential surface in Figure 2. On the singlet surface, all reaction channels involve significant barriers, ranging from 11.8 to 48.6 kcal/mol. The reaction prefers to occur on the triplet surface because the hydrogen abstraction pathway is effectively barrierless and highly exothermic. Moreover, because the intermediate wells IM1 and IM2 are similar in depth, the nascent collision complex can sample the two wells and will prefer to exit from IM1 via a lower barrier. Therefore, it should be

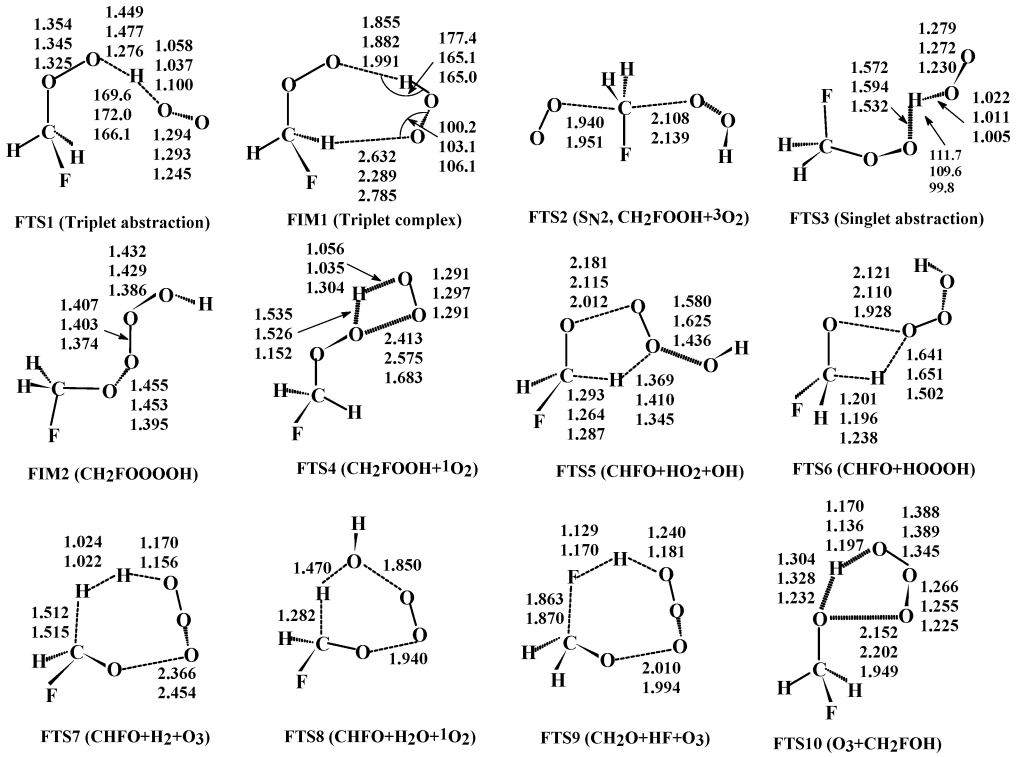

Figure 3. Optimized geometries of the transition states and intermediates involved in the $HO_2 + CH_2FOO$ reaction at various levels of theory. For the structures with three entries, from top to bottom, the data are obtained at the B3LYP/6-31G(d), B3LYP/6-311G(d,p), and CISD/cc-pVDZ levels, respectively. For the structures with two entries, the data are obtained at the B3LYP/6-31G(d) and B3LYP/6-311G(d,p) levels, respectively. The parameters for FTS8 are obtained at the MP2/6-31G(d) level. The bond distances are in angstroms, and the angles are in degrees.

unambiguous to deduce that the formation of $CH_3OOH + O_2$ is the dominant product channel in the $HO_2 + CH_3O_2$ reaction, in agreement with the experimental result in which CH_3OOH is the only product that could be detected.[3,4]

The isotope effect has been studied as well for the $HO_2 + CD_3OO$ reaction. As shown in Table 2, although the zero-point energy for each structure decreases because of D-substitution, the relative order of the barriers does not change; that is, the D-substitution does not affect the relative yields of the products. The hydrogen abstraction path on the triplet surface still exhibits the lowest barrier and remains the dominant reaction channel. In fact, it has been shown that CD_3OOH is the only product observed experimentally for the $HO_2 + CD_3OO$ reaction.[5]

III.2. The $HO_2 + CH_2FO_2$ Reaction. The structures of the intermediates and transition states of the $HO_2 + CH_2FO_2$ reaction are shown in Figure 3. The schematic potential energy surface is shown in Figure 4. The energetic data are summarized in Table 3. Similar to the $CH_3O_2 + HO_2$ reaction, the $CH_2FO_2 + HO_2$ reaction occurs on both singlet and triplet surfaces. The product channels involving transition states FTS2, FTS7, and FTS8 are ruled out in view of their significant barriers.

III.2.1. The Triplet Surface. A direct hydrogen abstraction path leads to CH_2FOOH and the triplet O_2 molecule. As shown in Figure 3, the intermediate well FIM1 exists in the entrance channel. FIM1 is a seven-membered-ring complex with two hydrogen bonds of 1.882 and 2.289 Å, respectively. The well depth is 8.89 kcal/mol. The formation of $CH_2FOOH + {}^3O_2$ proceeds via transition state FTS1. The forming O···H bond is 1.477 Å, while the breaking O···H bond is stretched to 1.037 Å, which is only ~0.07 Å longer than that of HO_2. The energy of FTS1 is slightly lower than that of the reactants by ~2.0 kcal/mol. As a result, the overall abstraction becomes essentially barrierless. In addition, the abstraction is exothermic by 43.24 kcal/mol. Therefore, it is conceivable that the abstraction should be facile both kinetically and thermodynamically.

No other reaction path could be found on the triplet surface. The optimization of the triplet CH_2FO_4H leads to the separation of CH_2FO_2 and HO_2, as shown in Figure 5 (upper panel). Note that at the B3LYP/6-311G(d,p) level the optimization finally leads to the hydrogen-bonded complex FIM1. Furthermore, the OO addition entrance channel complex was checked through a potential surface scan. Because of the multireference character of the reaction path, the complete active space (CAS) self-consistent field (SCF) calculation[37−41] was performed with the qualitatively accurate basis set 6-31G(d). The active space included six electrons and six orbitals. The result is shown in Figure 5 (lower panel). It is obvious that the terminal oxygen atom approach is repulsive on the triplet surface, whereas it is attractive on the singlet surface, as will be detailed below.

III.2.2. The Singlet Surface. As shown in Figure 4, the singlet surface is more complicated than the triplet one. The first reaction path is the hydrogen abstraction via transition state FTS3 with the formation of CH_2FOOH and the singlet O_2 molecule. The singlet abstraction is different from the triplet one in two repects. First, there is no weakly bound complex. Second, the O···H···O bond angle is much more bent (e.g., 109.6° in FTS3 vs 172.0° in FTS1). The barrier for abstraction is 7.31 kcal/mol.

All the remaining reactions precede via an addition/elimination mechanism. The initial adduct is the tetroxide intermediate, denoted as FIM2 in Figure 3. FIM2 is a nonplanar structure. The four oxygen atoms are twisted by 92.2°. The intermediate well depth is 14.13 kcal/mol, which is ~5 kcal/mol lower than that of the FIM1 complex.

Starting from FIM2, transition states FTS4, FTS6, FTS9, and FTS10, leading to $CH_2FOOH + {}^1O_2$, CHFO + HOOOH, $CH_2O + HF + O_3$, and $CH_2FOH + O_3$, respectively, exhibit similar barrier heights, namely, 7−9 kcal/mol. As shown in Figure 3, the four transition states have ring structures. For example, both FTS4 and FTS6 have four-membered rings and FTS9 and

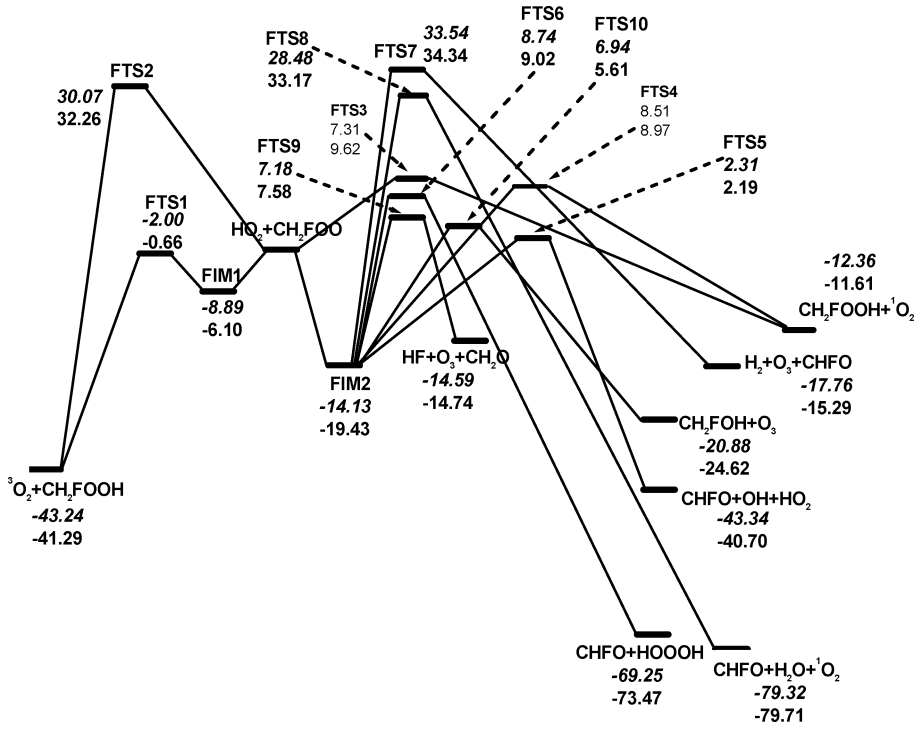

Figure 4. Schematic profile for the potential energy surface of the $HO_2 + CH_2FOO$ reaction. The indicated energies (in kilocalories per mole) are calculated with the CCSD(T)/cc-pVDZ//B3LYP/6-311G(d,p) scheme (upper) and the CCSD(T)/CBS2 scheme (lower), respectively.

TABLE 3: Relative Energies Calculated at Various Levels of Theory for the $HO_2 + CH_2FOO$ Reaction[a]

species	ZPE	B3LYP/ BS1[b]	MP2/ BS1	QCISD/ BS1	QCISD(T)/ BS1	CCSD(T)/ BS1	CCSD(T)/ BS2[c]	CCSD(T)/ BS3[d]	CCSD(T)/ CBS1[e]	CCSD(T)/ CBS2[f]
$HO_2 + CH_2FO_2$	31.33	0.0	0.0	0.0	0.0	0.0	0.0	0.0	0.0	0.0
FIM1	33.28	−8.35	−7.43	−6.83	−7.64	−7.61	−8.89	−7.12	−6.38	−6.10
FTS1	31.39	−7.31	−0.53	0.1	−1.26	−1.26	−2.00	−1.15	−0.80	−0.66
FTS2	31.14	20.45	42.76	35.83	31.23	31.80	30.07	31.46	32.04	32.26
FTS3	32.41	22.22	0.1	31.05	11.29	8.25	7.31	8.94	9.62	9.88
FIM2	34.18	−11.59	−23.13	−7.02	−13.50	−13.55	−14.13	−17.50	−18.92	−19.43
FTS4	32.55	15.97	−9.40	27.89	10.67	9.89	8.51	8.83	8.97	9.02
FTS5	30.13	3.81	−17.11	21.68	3.34	4.01	2.31	2.23	2.20	2.19
FTS6	30.59	12.41	−3.81	30.13	10.27	10.55	8.74	8.92	8.99	9.02
FTS7	26.95	36.50	19.73	36.44	34.94	35.73	33.54	34.05	34.26	34.34
FTS8[g]	31.51		12.56	52.44	27.95	32.39	28.48	31.46	32.71	33.17
FTS9	29.98	4.95	2.86	24.72	11.76	10.29	7.18	7.44	7.54	7.58
FTS10	30.59	10.92	−1.0.39	25.43	8.43	8.86	6.94	6.09	5.73	5.61
$CH_2FOOH + {}^3O_2$	32.41	−38.69	−57.10	−39.84	−42.67	−43.02	−43.24	−42.00	−41.49	−41.29
$CH_2FOOH + {}^1O_2$	32.39	0.31	−25.24	−6.53	−11.90	−12.40	−12.36	−11.89	−11.69	−11.61
$CHFO + HO + HO_2$	27.22	−38.22	−50.86	−44.49	−44.04	−44.10	−43.34	−41.66	−40.96	−40.70
CHFO + HOOOH	32.09	−65.98	−84.52	−65.56	−70.13	−70.21	−69.25	−71.93	−73.07	−73.47
$CHFO + H_2 + O_3$	23.94	−7.27	−41.14	−4.48	−18.13	−17.55	−17.76	−16.19	−15.53	−15.29
$CHFO + H_2O + O_2$	28.76	−64.99	−98.72	−81.02	−76.21	−80.74	−79.32	−79.57	−79.68	−79.71
$CH_2O + HF + O_3$	27.06	−1.16	−38.38	−3.29	−15.76	−15.43	−14.59	−14.69	−14.73	−14.74
$CH_2FOH + O_3$	32.80	−11.80	−44.98	−10.02	−22.17	−21.89	−20.88	−23.26	−24.26	−24.62

[a] In kilocalories per mole. The total energy of the reactants $HO_2 + CH_2FOO$ is as follows (in hartrees): −440.481 819 (B3LYP/BS1), −439.536 672 (MP2/BS1), −439.475 879 (QCISD/BS1), −439.506 244 [QCISD(T)/BS1], −439.504 092 [CCSD(T)/BS1], −439.338 545 [CCSD(T)/BS2], −439.787 570 [CCSD(T)/BS3], −439.976 63 [CCSD(T)/CBS1], −440.045 04 [CCSD(T)/CBS2]. [b] BS1 = 6-311G(d,p). [c] BS2 = cc-pVDZ. [d] BS3 = cc-pVTZ. [e] Using the formula in ref 35. [f] Using the formula in ref 36. [g] The MP2/6-31G(d) optimized geometry.

FTS10 have seven- and five-membered rings, respectively. The formation of the ringlike structures is helpful to disperse electrons and then weaken the bonding. As a result, such a structure has lower energy. However, these barriers are still well above the available energy at normal temperatures. Only at higher temperatures could these four channels play an observable role in the overall reaction, and they are thus not discussed further.

Among the possible pathways leading to fluorinated formaldehyde (CHFO), the reaction $HO_2 + CH_2FO_2 \rightarrow$ FIM2 $\rightarrow$ FTS5 $\rightarrow$ CHFO + OH + HO_2 involves the lowest barrier. The energy of FTS5 is only slightly higher than that of the reactants by 2.3 kcal/mol, which corresponds to ∼4 *RT* at room temperature. This implies that the barrier becomes essentially zero after thermal correction. Moreover, the overall reaction is highly exothermic by 43.34 kcal/mol. As shown in Figure 3, FTS5 has a five-membered-ring geometry. One of the hydrogen atoms is shifting from C to O, and simultaneously, the two OO bonds are breaking. The CO bond is shortened to be double-bond-like to give the product CHFO. It is interesting to note that this reaction appears to be a HO_2-catalyzed decomposition of the CH_2FOO radical because HO_2 is reproduced as one of the final products.

Experimentally, it was found that at room temperature the yield of CHFO accounts for almost 70% of products, while the

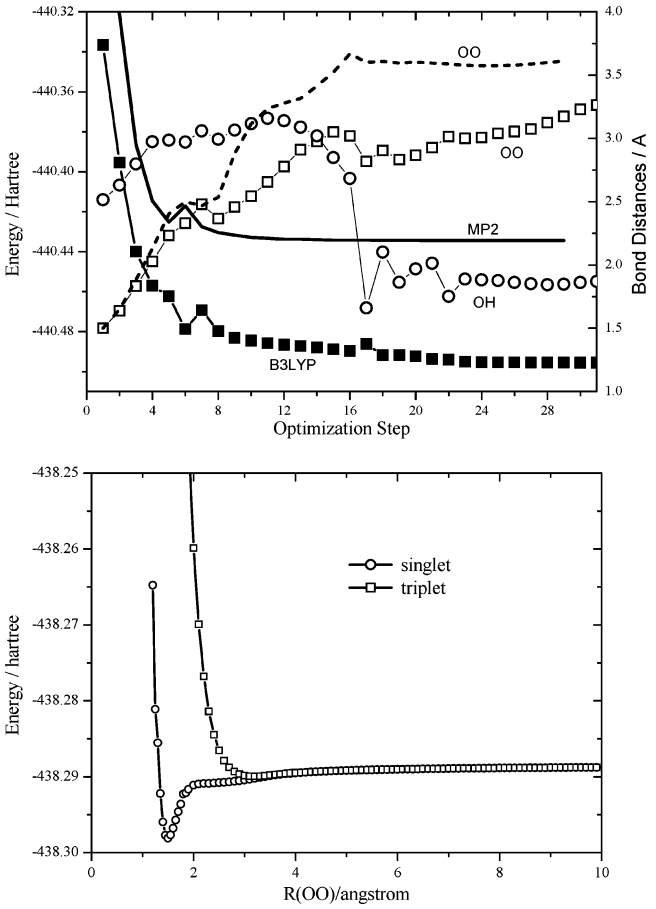

Figure 5. Potential energy profile for the OO addition entrance channel in the reaction of HO_2 with CH_2FOO. (upper panel) Energy and geometric profiles in the B3LYP (symbols + lines) and MP2 (lines) optimization with the 6-311G(d,p) basis set. OO means the distance between two approaching oxygen atoms, and OH means the distance between the H atom of HO_2 and the terminal O atom of CH_2FOO. (lower panel) The triplet and singlet entrance energy profiles at the CAS(6,6)/6-31G(d) level of theory. To obtain smooth energy curves, in the partial optimization, the CH_2F group is fixed to avoid rotation and only the three most important bond distances, C−O, O−O, and O−O, in the COOO skeleton are optimized. The step sizes are set to be 0.05 and 0.1 Å for R(O−O) < 1.9 Å and 1.9 Å < R(O−O) <10.0 Å, respectively, where R(O−O) means the distance between the two approaching O atoms.

branching to CH_2FOOH is only 30%.[11] The formation of CHFO and CH_2FOOH exhibits the lowest barrier on the singlet and triplet surfaces, respectively. Although FTS5 is somewhat higher than FTS1 in energy, both channels are effectively barrierless at room temperature. Moreover, the relative depths of the intermediate wells FIM1 and FIM2 have an influence on the reaction. The nascent collision complex can sample the two wells and will prefer to spend time as FIM2 because it is much deeper than FIM1. This effect could easily shift the product distribution in the CHFO direction. In addition, in the sense of transition state theory, besides the activation barrier, the pre-exponential factor A also needs to be taken into account. In this regard, FTS5 leading to CHFO should have a clear advantage because it is a ring structure. Therefore, our calculation supports that the yield of CHFO should be higher than that of CH_2FOOH, which is in agreement with the experimental result. Detailed kinetic modeling is necessary to obtain a more quantitative conclusion.

III.3. Unimolecular Decomposition of CH_3OOH and CH_2FOOH. The motivation to study the unimolecular decomposition of ROOH (R═CH_3, CH_2F) originates from Figures 2 and 4. It is noted that the abstraction reaction forming ROOH on the triplet surface is highly exothermic by around 40 kcal/mol. It is supposed that most of the available energy goes into the internal energy of the ROOH molecule, and thus makes ROOH vibrationally excited and reactive. This postulation results from the fact that the abstraction transition state is an early barrier and, empirically, the product might be internally excited in a reaction involving an early barrier. For example, in FTS1, the forming OH bond is 1.477 Å, which is ~1.5 times longer than the equilibrium value in CH_2FOOH. Consequently, ROOH might decompose further and thus affect the product distribution in the HO_2 + RO_2 reaction.

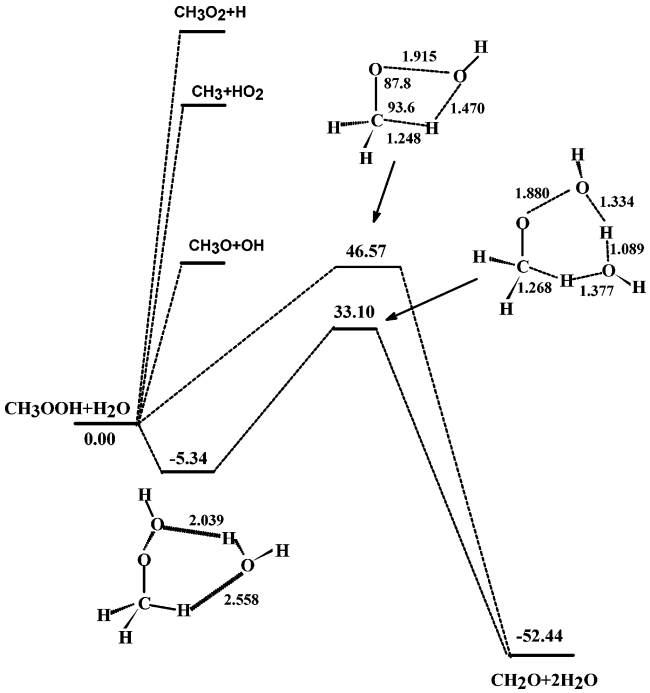

Figure 6. Decomposition pathways for the CH_3OOH molecule. The indicated energies (in kilocalories per mole) are calculated with the CCSD(T)/cc-pVDZ//B3LYP/6-311G(d,p) scheme.

The following dissociation channels have been calculated at the CCSD(T)/cc-pVDZ//B3LYP/6-311G(d,p) level of theory for CH_3OOH* and CH_2FOOH*, respectively.

$$CH_3OOH^* \rightarrow CH_2O + H_2O \quad \Delta_rH^\circ_0 = -51.5 \pm 1.9 \text{ kcal/mol} \quad \text{(R1a)}$$

$$\rightarrow CH_3O + OH \quad \Delta_rH^\circ_0 = 45.6 \pm 2.9 \text{ kcal/mol} \quad \text{(R2a)}$$

$$\rightarrow CH_3O_2 + H \quad \Delta_rH^\circ_0 = 87.5 \pm 3.1 \text{ kcal/mol} \quad \text{(R3a)}$$

$$\rightarrow CH_3 + HO_2 \quad \Delta_rH^\circ_0 = 70.7 \pm 2.8 \text{ kcal/mol} \quad \text{(R4a)}$$

where the $\Delta_rH^\circ_0$ values are obtained using the experimental enthalpies of formation taken from ref 33 with a thermal correction.

$$CH_2FOOH^* \rightarrow CHFO + H_2O \quad \text{(R1b)}$$

$$\rightarrow CH_2O + FOH \quad \text{(R2b)}$$

$$\rightarrow CH_2FO + OH \quad \text{(R3b)}$$

$$\rightarrow CH_2FO_2 + H \quad \text{(R4b)}$$

$$\rightarrow CH_2F + HO_2 \quad \text{(R5b)}$$

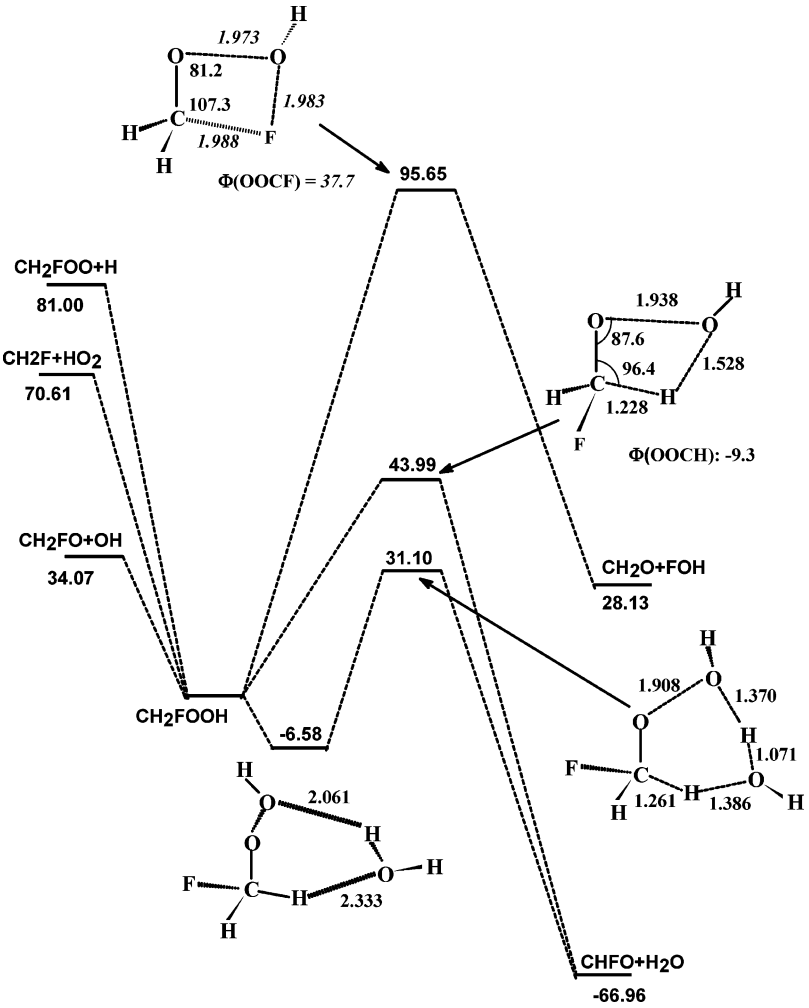

Figure 7. Decomposition pathways for the CH_2FOOH molecule. The indicated energies (in kilocalories per mole) are calculated with the CCSD(T)/cc-pVDZ//B3LYP/6-311G(d,p) scheme. Note that the channel $CH_2FOOH \rightarrow CH_2O+FOH$ is calculated at the CCSD(T)/cc-pVDZ//MP2/6-311G(d,p) level because the transition state cannot be found with the B3LYP/6-311G(d,p) method.

The results (e.g., structures and energies) are shown in Figures 6 and 7, respectively. As for the decomposition of CH_3OOH, the R1a channel has the lowest barrier, 46.57 kcal/mol. This value is higher than the total available energy of ~38 kcal/mol released in the abstraction process. Even if all the available energy goes into the internal energy of CH_3OOH^*, it is still not enough to break CH_3OOH into CH_2O. All the other decomposition channels leading to radical products are highly endothermic. Therefore, most CH_3OOH^* should be deactivated through collision. However, it is worth noting that the product H_2O molecule may initialize an autocatalytic process. The H_2O molecule could serve as a catalyst to lower the barrier for R1a significantly. As shown in Figure 6, the H_2O-mediated dissociation of CH_3OOH to $CH_2O + H_2O$ only needs to overcome a barrier of 33.1 kcal/mol. This value is already ~5 kcal/mol less than the available energy of 38 kcal/mol.

For the CH_2FOOH molecule, the most favorable reaction is R3b with a barrier of 34.07 kcal/mol. It has been shown that the CH_2FO radical decomposes further to give predominantly CHFO and H.[42] The other important channel is R1b. The barrier of 43.99 kcal/mol is very close to the available energy (i.e., 43.24 kcal/mol). Moreover, R1a is highly exothermic. It is conceivable that a fraction of CH_2FOOH^* may decompose into CHFO once it is formed in the $HO_2 + CH_2FOO$ reaction. Analogous to R1a, the H_2O molecule could serve as a catalyst to accelerate the dissociation of CH_2FOOH via R1b. As shown in Figure 7, the barrier is lowered by 12.89 kcal/mol.

III.4. Conformers of the Tetroxides CH_3O_4H and CH_2FO_4H. The tetroxide RO_4H is an important intermediate in the $HO_2 + RO_2$ reaction. All conformers of the O_4 backbone of RO_4H have been explored for both CH_3O_4H and CH_2FO_4H, together with the internal rotation transition states. The structures and relative energies are shown in Figures 8 and 9 for CH_3O_4H and CH_2FO_4H, respectively. The energies of the conformers are very close to each other. However, there are relatively large barriers between two conformers. There is no measurement of the enthalpies of formation for CH_3O_4H and CH_2FO_4H reported in the literature. Using the standard G3MP2//B3LYP/6-31G* scheme,[43] the enthalpies of formation for the most stable CH_3O_4H and CH_2FO_4H conformers have been calculated: $\Delta_f H^\circ_0(CH_3O_4H) = -4.3$ kcal/mol and $\Delta_f H^\circ_0(CH_2FO_4H) = -55.6$ kcal/mol. Additionally, the enthalpies of CH_2FOOH and CH_3OOH are calculated to be -78.1 and -26.9 kcal/mol, respectively. The value for CH_3OOH is in agreement with the experimental value of -29.2 ± 2.4 kcal/mol.[33] An error of ± 2.4 kcal/mol is estimated for the theoretical values.

III.5. Validation of the Computational Methods Employed in the Study. The CCSD(T)/cc-pVDZ//B3LYP/6-311G** level of theory is employed in the present systematic study. The reliability of such computations has been validated and calibrated through more extensive calculations on the $HO_2 + CH_2FO_2$ reaction. For comparison, the geometrical parameters optimized at the B3LYP/6-31G(d), B3LYP/6-311G(d,p), and CISD/cc-pVDZ levels are shown in Figure 3. It is noted that the

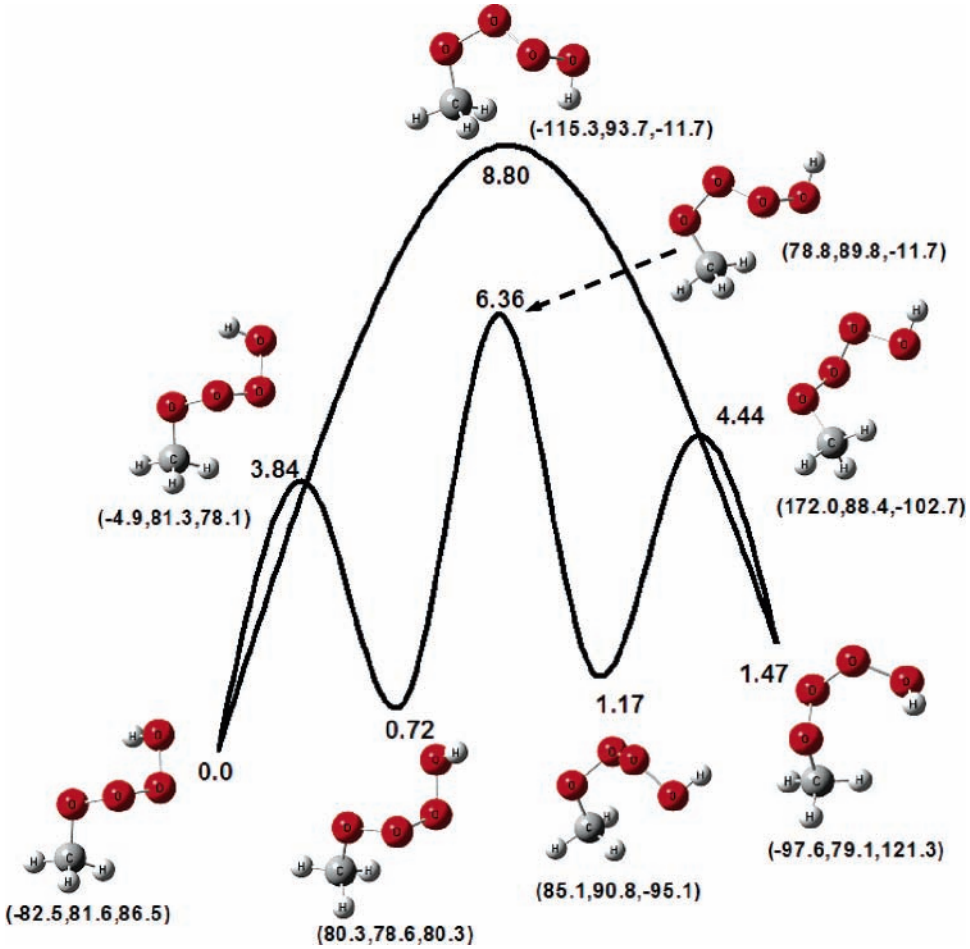

Figure 8. CH_3O_4H conformers and the corresponding transition states for their interconversion. The geometries are optimized at the B3LYP/6-311G(d,p) level, and the indicated energies (in kilocalories per mole) are calculated at the CCSD(T)/cc-pVDZ level. The values in brackets are three dihedral angles, namely, ϕ(HOOO), ϕ(OOOO), and ϕ(OOOC).

geometries do not change dramatically with the different levels of theory except for one transition state (FTS4). Moreover, with the B3LYP method, the basis set 6-311G(d,p) appears to be adequate. In fact, B3LYP/6-311G(d,p) has been widely used to study reactions involving open-shell radicals because of its good performance in geometrical optimization and in annihilation of spin contamination.[44] However, higher levels of theory have to be used to improve the quality of the energies, especially the relative energies of barrier heights and reaction heats.

Table 3 summarizes the energies relative to the reactants (HO_2 + CH_2FO_2) calculated at various levels of theory including MP2/6-311G(d,p), QCISD/6-311G(d,p), QCISD(T)/6-311G(d,p), CCSD(T)/6-311G(d,p), CCSD(T)/cc-pVDZ, and CCSD(T)/cc-pVTZ. Moreover, the last two CCSD(T) energies are extrapolated to the complete basis set (CBS) limit using the two-point (i.e., cc-pVDZ and cc-pVTZ) formula.[35,36] Obviously, the data obtained at the lower levels such as B3LYP/6-311G(d,p) and MP2/6-311G(d,p) are significantly different from the CCSD(T)/CBS results. However, the results obtained at the CCSD(T)/cc-pVDZ level are very close to the CCSD(T)/CBS data for most species. Comparing a total of 20 relative energies at the CCSD(T)/cc-pVDZ level with those at the CCSD(T)/CBS level in Table 3, we found that the mean absolute deviation is 1.74 kcal/mol with the errors ranging from 0.11 to 4.79 kcal/mol. The results obtained at the CCSD(T) level with the triple-ζ basis sets 6-311G(d,p) and cc-pVTZ are slightly better; however, the improvement is not significant in comparison with the CCSD(T)/cc-pVDZ data but the computational cost increases dramatically. Therefore, as a balance between accuracy and cost, the CCSD(T)/cc-pVDZ method should be a reasonable level for calculating the relative energies. For example, as can be seen in Table 3, the calculated heats of reaction are in good agreement with the experimental data,[33,34] which is an indication of the good performance of the CCSD(T)/cc-pVDZ//B3LYP/6-311G(d,p) method.

Table 4 shows the dependence of the relative energies on the geometries optimized at different levels of theory. It is clear that the absolute values of energies do change more or less with the geometries. The most dramatic deviation is seen in the CCSD(T)/cc-pVDZ energies of FTS4 between the B3LYP/6-311G(d,p) and CISD/cc-pVDZ geometries. It should be noted that the CCSD(T)/cc-pVDZ//CISD/cc-pVDZ energy is an artifact because of an internal failure of the CCSD(T) calculation. Fortunately, the relative order of most species does not change and basically remains the same at different levels, which indicates that the errors in the energies are systematic.

IV. Concluding Remarks

The present paper reports an ab initio study on the reactions of HO_2 with CH_3O_2 and CH_2FO_2. The major features of the reaction mechanisms for both reactions have been clarified at a relatively reliable level of theory. A few conclusions can be drawn as follows:

(1) Both the HO_2 + CH_3OO and the HO_2 + CH_2FOO reactions have a simpler triplet potential energy surface on which the hydrogen abstraction path is effectively barrierless and a more complicated singlet surface on which the addition/elimination mechanism dominates.

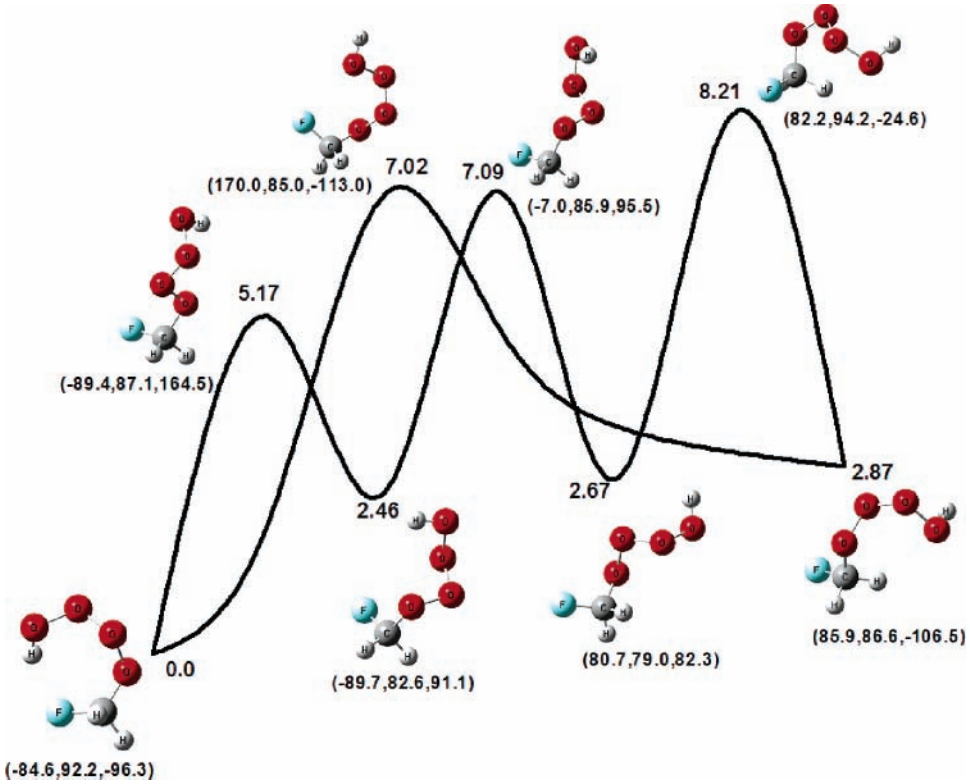

Figure 9. CH_2FO_4H conformers and the corresponding transition states for their interconversion. The geometries are optimized at the B3LYP/6-311G(d,p) level, and the indicated energies (in kilocalories per mole) are calculated at the CCSD(T)/cc-pVDZ level. The values in brackets are three dihedral angles, namely, ϕ(HOOO), ϕ(OOOO), and ϕ(OOOC).

TABLE 4: Comparison between the Relative Energies with Respect to the HO_2 + CH_2FOO Reactants Calculated Using the Optimized Geometries at Different Levels of Theory[a]

species	QCISD(T)/ 6-31G*// B3LYP/ 6-31G*	G3(MP2)// B3LYP/ 6-31G*	CCSD(T)/ cc-pVDZ// CISD/ cc-pVDZ	CCSD(T)/ cc-pVDZ// B3LYP/ 6-311G**	CCSD(T)/ CBS1// B3LYP/ 6-311G**
FIM1	−10.16	−6.65	−5.28	−8.89	−6.38
FIM2	−18.44	−18.07	−11.68	−14.13	−18.92
FTS1	0.96	0.85	−3.41	−2.00	−0.80
FTS2	30.55	31.27		30.07	32.04
FTS3	10.68	11.25	18.18	7.31	9.62
FTS4	40.97 [b]	36.86 [b]	36.47	8.51	8.97
FTS5	6.71	−1.22	8.48	2.31	2.20
FTS6	10.97	5.25	16.36	8.74	8.99
FTS7	42.92	32.89		33.54	34.26
FTS8	28.17	23.28		28.48	32.71
FTS9	10.51	4.93		7.18	7.54
FTS10	10.62	6.10	12.40	6.94	5.73

[a] In kilocalories per mole. The symbol A//B represents that the single-point energy is calculated at the A level with the geometry optimized at the B level. [b] Calculated with the CISD/6-31G* geometry.

(2) A simple explanation of the F-substituted effect can be offered. Without the substitution, the reaction proceeds only on the triplet surface through hydrogen abstraction. The reaction paths on the singlet surface cannot be competitive because of significant barriers. After the F-substitution, some barriers on the singlet surface are lowered. As a result, more product channels become open. Moreover, the deeper well in the singlet entrance channel (compared with that on the triplet surface) gives an advantage to the production of carbonyl compounds. Thus, under normal experimental conditions, for the HO_2 + CH_3OO reaction, CH_3OOH is the dominant product. For the HO_2 + CH_2FOO reaction, both CH_2FOOH and CHFO are observable products, while the latter is dominant.

(3) The secondary decomposition of CH_3OOH and CH_2-FOOH may generate additional carbonyl products (CH_2O or CHFO). Water could act as a catalyst in the unimolecular decomposition.

(4) For a systematic computational study on the HO_2 + RO_2 reaction, the scheme CCSD(T)/cc-pVDZ // B3LYP/6-311G(d,p) has the desired balance between cost and good performance.

In our further study, the minimum energy reaction paths (MREPs) obtained in the present study will be employed to carry out detailed kinetic modeling to predict the temperature and pressure dependence of the rate constants and the branching ratios of the products.

Acknowledgment. This work is supported by the Foundation for the Author of National Excellent Doctoral Dissertation of China. We would like to thank Prof. James T. Muckerman of Brookhaven National Laboratory for improving the English of the manuscript.

References and Notes

(1) Wallington, T. J.; Dagaut, P.; Kurylo, M. J. *Chem. Rev.* **1992**, *92*, 667.
(2) Orlando, J. J.; Tyndall, G. S.; Wallington, T. J. *Chem. Rev.* **2003**, *103*, 4657.
(3) Wallington, T. J.; Japar, S. M. *Chem. Phys. Lett.* **1990**, *167*, 513.
(4) Wallington, T. J. *J. Chem. Soc., Faraday Trans.* **1991**, *87*, 2379.
(5) Wallington, T. J.; Hurley, M. D. *Chem. Phys. Lett.* **1992**, *193*, 84.
(6) Wallington, T. J.; Japar, S. M. *Chem. Phys. Lett.* **1990**, *166*, 495.
(7) Spittler, M.; Barnes, I.; Becker, K. H.; Wallington, T. J. *Chem. Phys. Lett.* **2000**, *321*, 57.
(8) Hasson, A. S.; Tyndall, G. S.; Orlando, J. J. *J. Phys. Chem. A* **2004**, *108*, 5979 and references therein.
(9) Rowley, D. M.; Lesclaux, R.; Lightfoot, P. D.; Noziere, B.; Wallington, T. J.; Hurley, M. D. *J. Phys. Chem.* **1992**, *96*, 4889.
(10) Rowley, D. M.; Lesclaux, R.; Lightfoot, P. D.; Hughes, K.; Wallington, T. J.; Hurley, M. D. *J. Phys. Chem.* **1992**, *96*, 7043.
(11) Wallington, T. J.; Hurley, M. D.; Schneider, W. F.; Sehested, J.; Nielsen, O. J. *Chem. Phys. Lett.* **1994**, *218*, 34.

(12) Wallington, T. J.; Hurley, M. D.; Schneider, W. F. *Chem. Phys. Lett.* **1996**, *251*, 164.

(13) Catoire, V.; Lesclaux, R.; Schneider, W. F.; Wallington, T. J. *J. Phys. Chem.* **1996**, *100*, 14356.

(14) Burrows, J. P.; Moortgat, G. K.; Tyndall, G. S.; Cox, R. A.; Jenkin, M. E.; Hayman, M. D.; Veyret, B. *J. Phys. Chem.* **1989**, *93*, 2375.

(15) Wallington, T. J.; Hurley, M. D.; Ball, J. C.; Jenkin, M. E. *Chem. Phys. Lett.* **1993**, *211*, 41.

(16) Niki, H.; Maker, P. D.; Savage, C. M.; Breitenbach, L. P. *J. Phys. Chem.* **1985**, *89*, 588.

(17) Moortgat, G. K.; Veyret, B.; Lesclaux, R. *Chem. Phys. Lett.* **1989**, *160*, 443.

(18) Horie, O.; Moortgat, G. K. *J. Chem. Soc., Faraday Trans.* **1992**, *88*, 3305.

(19) Crawford, M. A.; Wallington, T. J.; Szente, J. J.; Maricq, M. M.; Francisco, J. S. *J. Phys. Chem. A* **1999**, *103*, 365.

(20) Tomas, A.; Villenave, E.; Lesclaux, R. *J. Phys. Chem. A* **2001**, *105*, 3505.

(21) Tyndall, G. S.; Cox, R. A.; Granier, C.; Lesclaux, R.; Moortgat, G. K.; Pilling, M. J.; Ravishankara, A. R.; Wallington, T. J. *J. Geophys. Res. D* **2001**, *106*, 12157.

(22) Sulback Anderson, M. P.; Hurley, M. D.; Wallington, T. J.; Ball, J. C.; Martin, J. W.; Ellis, D. A.; Maburg, S. A. *Chem. Phys. Lett.* **2003**, *381*, 14.

(23) (a) Becke, A. D. *J. Chem. Phys.* **1993**, *98*, 5648. (b) Lee, C.; Yang, W.; Parr, R. G. *Phys. Rev. B* **1988**, *37*, 785.

(24) Gonzalez, C.; Schlegel, H. B. *J. Phys. Chem.* **1989**, *90*, 2514.

(25) Foresman, J. B.; Frisch, A. E. *Exploring Chemistry with Electronic Structure Methods*, 2nd ed.; Gaussian, Inc.; Pittsburgh, PA, 1996; p 173.

(26) Shaik, S. S.; Schlegel, H. B.; Wolfe, S. *Theoretical Aspects of Physical Organic Chemistry: The S_N2 Mechanism*; Wiley: New York, 1992; pp 50−51.

(27) Raghavachari, K.; Pople, J. A. *Int. J. Quantum Chem.* **1981**, *20*, 167.

(28) Gauss, J.; Cremer, C. *Chem. Phys. Lett.* **1988**, *150*, 280.

(29) Salter, E. A.; Trucks, G. W.; Bartlett, R. J. *J. Chem. Phys.* **1989**, *90*, 1752.

(30) Pople, J. A.; Krishnan, R.; Schlegel, H. B.; Binkley, J. S. *Int. J. Quantum Chem.* **1978**, *14*, 545.

(31) Bartlett, R. J.; Purvis, G. D. *Int. J. Quantum Chem.* **1978**, *14*, 516.

(32) Frisch, M. J.; et al. *Gaussian 03*, revision B.05; Gaussian Inc.: Pittburgh, PA, 2003.

(33) Sander, S. P.; et al. *Chemical Kinetics and Photochemical Data for Use in Atmospheric Studies*, JPL Publication 02-25, Evaluation Number 14, **2003**, Appendix A-1.

(34) Speranza, M. *Inorg. Chem.* **1996**, *35*, 6140.

(35) Kutzelnigg, W.; Morgan, J. D., III. *J. Chem. Phys.* **1992**, *96*, 4484.

(36) Huh, S. B.; Lee, J. S. *J. Chem. Phys.* **2003**, *118*, 3035.

(37) Hegarty, D.; Robb, M. A. *Mol. Phys.* **1979**, *38*, 1795.

(38) Werner, H. J.; Knowles, P. J. *J. Chem. Phys.* **1985**, *82*, 5053.

(39) Mcdouall, J. J.; Peasley, K.; Robb, M. A. *Chem. Phys. Lett.* **1988**, *148*, 183.

(40) Werner, H. J. *Mol. Phys.* **1996**, *89*, 645.

(41) Werner, H. J.; Knowles, P. J. *J. Chem. Phys.* **1988**, *89*, 5803.

(42) Wang, B.; Hou, H.; Gu, Y. *Chem. Phys. Lett.* **1999**, *304*, 278.

(43) Baboul, A. G.; Curtiss, L. A.; Redfern, P. C.; Raghavachari, K. *J. Chem. Phys.* **1999**, *110*, 7650.

(44) For example, see: Mebel, A. M.; Morokuma, K.; Lin, M. C. *J. Chem. Phys.* **1995**, *103*, 7414.